Journal of Applied Physics

RESEARCH ARTICLE | NOVEMBER 17 2025

Determining electron inelastic mean free paths by iterative Monte Carlo analysis of the backscattered electron spectrum

Jiamin Gong ; Lihao Yang ; Hideki Yoshikawa; Shigeo Tanuma ; Bo Da ; Chuanhong Jin ; Zejun Ding

J. Appl. Phys. 138, 195301 (2025)
https://doi.org/10.1063/5.0302645

Journal of Applied Physics ARTICLE pubs.aip.org/aip/jap

Determining electron inelastic mean free paths by iterative Monte Carlo analysis of the backscattered electron spectrum

Cite as: J. Appl. Phys. **138**, 195301 (2025); doi: 10.1063/5.0302645
Submitted: 16 September 2025 · Accepted: 27 October 2025 ·
Published Online: 17 November 2025

View Online Export Citation CrossMark

Jiamin Gong,[1] Lihao Yang,[2,3] Hideki Yoshikawa,[4] Shigeo Tanuma,[5] Bo Da,[4,a)] Chuanhong Jin,[1] and Zejun Ding[2,3,a)]

AFFILIATIONS

[1]State Key Laboratory of Silicon and Advanced Semiconductor Materials, School of Materials Science and Engineering, Zhejiang University, Hangzhou, Zhejiang 310027, People's Republic of China
[2]Hefei National Research Center for Physical Sciences at the Microscale, University of Science and Technology of China, Hefei, Anhui 230026, People's Republic of China
[3]Department of Physics, University of Science and Technology of China, Hefei, Anhui 230026, People's Republic of China
[4]Center for Basic Research on Materials, National Institute for Materials Science, Tsukuba, Ibaraki 305-0044, Japan
[5]Materials Data Platform Center, National Institute for Materials Science, Tsukuba, Ibaraki 305-0044, Japan

[a)]**Authors to whom correspondence should be addressed:** DA.Bo@nims.go.jp and zjding@ustc.edu.cn

ABSTRACT

This study presents a novel method for extracting inelastic mean free paths (IMFPs) of electrons in solids from the backscattered electron spectrum (BES) using iterative Monte Carlo simulations. In our approach, the IMFP is parameterized using the Tanuma–Powell–Penn (TPP-2M) formula and a classical trajectory Monte Carlo simulation is used to model electron transport processes and generate a theoretical BES. Through an iterative process, we optimize the TPP parameters to achieve the best fit between the simulated and experimental spectra over a wide energy range. This method was applied to determine the IMFPs of 25 targets, such as C (graphite), Mg, Al (100), Al (111), Si, Ti, V, Cr, Fe, Co, Ni, Cu (100), Cu (110), Cu (111), Mo, Ru, Rh, Ag, Sn, W, Re, Ir, Pt, Au, and Bi, in the energy range from 200 to 4900 eV, using a comprehensive experimental BES data set. The results demonstrate that the IMFPs obtained with our BES method show an average root-mean-square deviation of approximately 15% from values calculated using the full-Penn algorithm and the standard TPP-2M formula. This approach not only provides a new technique for the IMFP measurement but also offers a novel perspective for utilizing the continuous background signal in surface electron spectroscopy, which is typically overlooked.

INTRODUCTION

The electron inelastic mean free path (IMFP) is a fundamental parameter that describes electron transport in solids and governs the surface sensitivity of core electron spectroscopy techniques.[1–3] Accurate IMFP values are, therefore, critical for quantitative analysis in x-ray photoelectron spectroscopy (XPS) and Auger electron spectroscopy (AES).[4–8] Over the years, several experimental and theoretical approaches have been developed to determine the IMFPs.

A widely used experimental technique is elastic peak electron spectroscopy (EPES),[4–11] which determines the IMFP by analyzing the intensity of elastically backscattered electrons. The method relies on comparing the elastic peak intensities of a sample to those of a reference material with a known IMFP value. Consequently, the accuracy of the resulting IMFP is directly dependent on the reliability of the reference data. While it requires such careful calibration and reference data, EPES provides a direct and robust experimental approach for IMFP determination.

Another common approach is the overlayer-film method,[12,13] where the attenuation of a substrate's photoemission or Auger signal is measured as a function of the thickness of a deposited

thin film. While straightforward, this technique typically yields an effective attenuation length (EAL) rather than the absolute IMFP,[14] which includes contributions from both inelastic and elastic scattering; however, to extract the true value of the IMFP, careful correction procedures are required.

Furthermore, reflection electron energy loss spectroscopy (REELS)[15–20] provides a powerful pathway to obtain the IMFP by determining the material's energy loss function (ELF).[21] The ELF, given by $\mathrm{Im}\{-1/\varepsilon(\omega)\}$, where $\varepsilon(\omega)$ is the optical dielectric function, governs the probability of inelastic scattering[22–26] and, thus, determines the IMFP.[27,28] The recently developed reverse Monte Carlo (RMC) method allows a highly accurate evaluation of the ELF from the experimentally measured REELS spectrum.[29–36] The REELS-RMC method, thus, provides an accurate approach to the IMFP determination by connecting experimental energy loss data to the material's dielectric response at the cost of extensive computation.

IMFP determination based on secondary electrons has also been proposed.[37] Secondary electrons are low-energy electrons (typically < 50 eV) excited by the incident electrons from the valence or conduction band in the material. Due to the low energy nature of the secondary electrons, their escape depth is strongly dependent on the IMFP of the material. By analyzing the energy distribution and angle distribution of secondary electrons, the IMFP may be derived.

While these methods utilize specific features of the electron energy spectrum—such as the elastic peak, characteristic photoemission lines, or discrete energy loss features—the broad, continuous background of backscattered electrons has remained largely unexploited for IMFP determination. This background signal contains rich information about the cumulative effects of inelastic scattering events that an electron undergoes before escaping a solid.

In this work, we present a novel approach that leverages this often-discarded BES to determine the IMFP. Our method combines experimental BES data (~200/300 eV to E_0−100 eV, where E_0 denotes the primary electron energy) with an iterative Monte Carlo simulation. We parameterize the IMFP using the Tanuma–Powell–Penn (TPP-2M) formula[38] and iteratively adjust its parameters until the simulated BES achieves an optimal fit with the experimental spectrum. A key innovation of our approach is the development of "artificial" ELFs. These artificial ELFs, each constructed to satisfy the fundamental physical sum rules, can be used for materials whose optical data are not available for calculating their true ELFs. As we will demonstrate, the resulting IMFP is robust and shows limited dependence on the precise shape of the ELF. This robustness enables reliable IMFP measurements for a wide range of materials, significantly expanding the applicability of experimental IMFP determination.

EXPERIMENT

Goto has performed an extensive experimental measurement of the BES data, which are employed in this study, for a variety of elemental solids with a cylindrical mirror analyzer (CMA) developed in the 1990s.[39,40] The electron gun, aligned coaxially with the CMA, ensures that electrons are incident perpendicular to the sample surface. The emission angle of the analyzer ranged between 36.3° and 48.3°, with respect to the surface normal. The incident

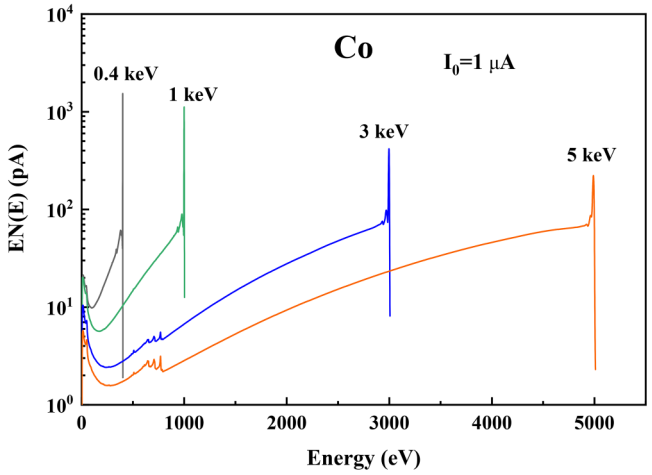

FIG. 1. The energy spectra of backscattered electrons measured at different primary energies for Co.

electron energy ranged from 400 to 5000 eV, with a beam current of ~1 μA. The spectra were collected in the $EN(E)$ mode, with an energy resolution of $f_e = \Delta E_s/E = 0.25\%$ and an energy step of 0.05 eV. Figure 1 shows the measured $EN(E)$ spectra of cobalt at incident electron energies of 0.4, 1, 3, and 5 keV.

THEORETICAL METHODS

Artificial optical ELF

In this study, we have employed the up-to-date classical trajectory Monte Carlo (CTMC) code[41] to simulate backscattered electron spectra. Specifically, the electron trajectories are tracked by sampling their step lengths, energy losses, and angular deflections according to the respective probability distributions. The electron-atom elastic scattering was described by Mott's cross section,[42] which determines the rate of elastic scattering and angular distribution of electrons in the scattering events. A dielectric functional approach is used to model electron inelastic scattering,[43] where the differential inverse inelastic mean free path (DIIMFP) governs the distribution of energy loss and momentum transfer during the inelastic scattering events. The key to a dielectric functional model lies in obtaining the momentum-dependent ELF, given by $\mathrm{Im}[-1/\varepsilon(q,\omega)]$. Here, the full-Penn algorithm (FPA) is used to extrapolate the optical ELF of the material into the q-ω plane.[28] For materials whose optical ELFs are unknown, we propose a method for constructing an artificial optical ELF as an approximation: a Drude-type formula is used to describe the ELF of a material in the energy loss range of 0–100 eV,

$$\mathrm{Im}\left[\frac{-1}{\varepsilon(\omega;\omega_p,\gamma=\omega_p)}\right]=\frac{A\omega\gamma\omega_p^2}{\left(\omega^2-\omega_p^2\right)^2+\omega^2\omega_p^2}, \quad (1)$$

where A, ω_p, and γ represent the amplitude, energy, and half-width of a Drude oscillator, respectively, and we have taken $\gamma = \omega_p$. For

the energy loss beyond 100 eV, the ELF is calculated using the atomic scattering factors from the Henke database[44] (100 eV–30 keV) and the EPDL97 database[45] (30 keV–10 MeV). Based on the two constraints of the *f*-sum rule and the *ps*-sum rule, one can derive the unique value for the parameters A and ω_p in Eq. (1) and thereby construct a Drude-type ELF. The *f*-sum rule and the *ps*-sum rule[23,46] are given, respectively, as

$$Z_{\text{eff}}|_{\text{ELF}} = \frac{2}{\pi\Omega_p^2}\int_0^\infty \omega \text{Im}[-1/\varepsilon(\omega)]d\omega = Z, \tag{2}$$

$$P_{\text{eff}}|_{\text{ELF}} = \frac{2}{\pi}\int_0^\infty \frac{1}{\omega}\text{Im}[-1/\varepsilon(\omega)]d\omega + \text{Re}[-1/\varepsilon(0)] = 1, \tag{3}$$

where $\hbar\Omega_p = \sqrt{4\pi n_a/m}$ and n_a is the atomic density and Z is the atomic number of the material.

Figure 2 presents a comparison between the artificial ELFs and the optical ELFs obtained from the literature[47] for the materials Au, Bi, Al, and Si.

In the Monte Carlo simulation, the IMFP of electrons, λ_{in}, is parameterized in the form of the modified Bethe equation (the TPP-2M formula) as follows:

$$\lambda_{\text{in}} = \frac{E}{E_p^2\left[\beta\ln(\gamma E) - \frac{C}{E} + \frac{D}{E^2}\right]}, \tag{4}$$

where E is the kinetic energy of an electron (with respect to the Fermi energy). $E_p = 28.8\sqrt{N_v\rho/M}$ is the plasmon energy of a free-electron metal, where N_v is the number of valence electrons per atom or molecule, ρ is the mass density of the bulk material, and M is the atomic mass. β, γ, C, and D are the parameters in the equation. Here, we only consider the BES for the electron energy larger than 200 eV so that the parameters C and D are inconsequential as previously reported.[48,49] Thus, we adopt only two parameters β and γ to describe the IMFP as follows:

$$\lambda_{\text{in}} = \frac{E}{E_p^2\beta\ln(\gamma E)}. \tag{5}$$

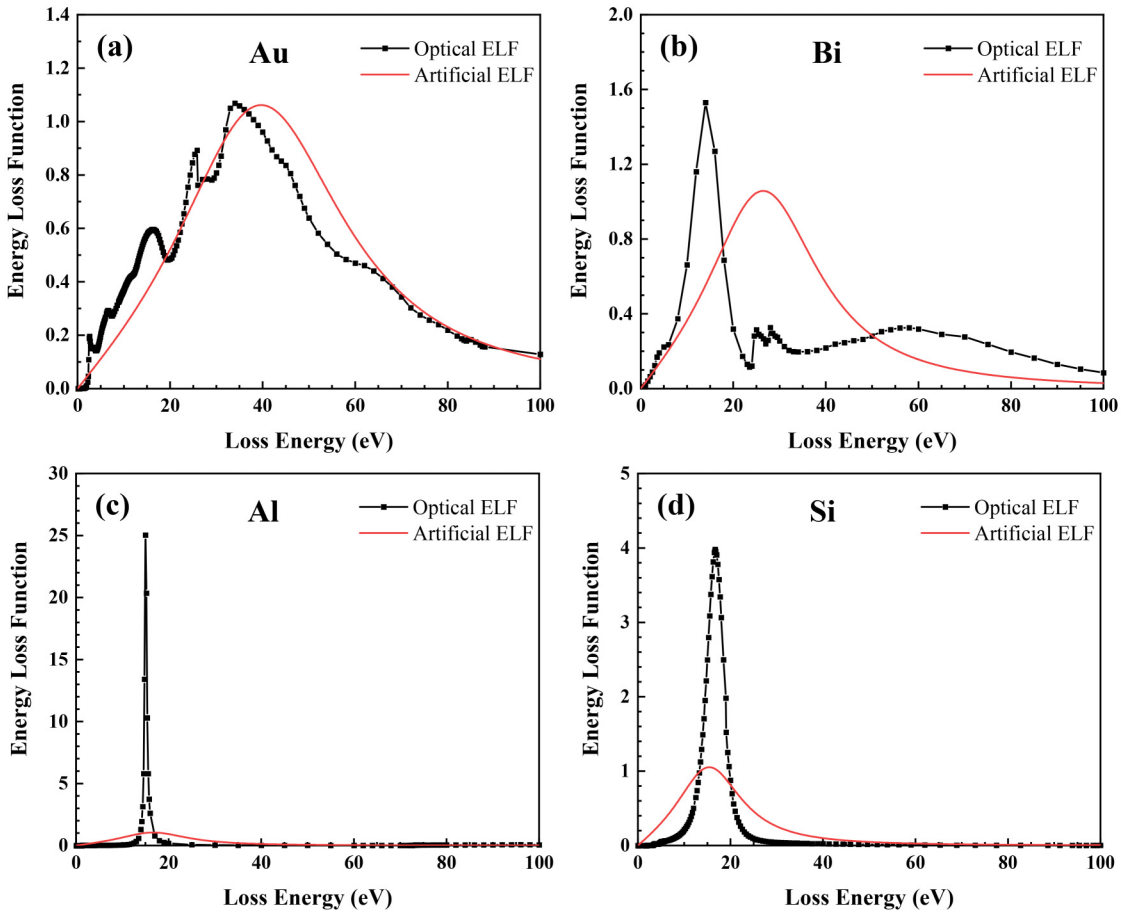

FIG. 2. The comparison of the optical ELFs (the black line) with the artificial ELFs (the red line) for (a) Au, (b) Bi, (c) Al, and (d) Si.

Extracting IMFP from BES

Based on the above analysis, the simulated current intensity $I_{sim}(E)$ can be obtained through a Monte Carlo simulation. To compare with the experimental BES data, it is necessary to convolute the simulated current intensity for the finite energy resolution with a Gaussian distribution function whose full width at half maximum (FWHM), ΔE_e, is expressed as follows:[6]

$$\Delta E_e = \sqrt{\Delta E_s^2 + \Delta E_g^2 + \Delta E_R^2}, \tag{6}$$

where ΔE_s is the energy resolution of the CMA, ΔE_g represents the inherent broadening of the electrons emitted from the electron gun, and ΔE_R is the intrinsic recoil broadening, which is the broadening of the elastic peak resulting from the energy loss due to the elastic scattering of electrons with surface atoms. Since we employ a relatively high incident electron energy (400–5000 eV) and only consider the spectrum in the energy range far away from the elastic peak, the primary factor influencing ΔE_e is ΔE_s, whereas the broadening effects caused by the electron gun and intrinsic recoil are minimal. Therefore, we take $\Delta E_e = \Delta E_s = f_e E$, which leads to the following equation:

$$\sigma = \frac{\Delta E_e}{2 \times \sqrt{2 \times \ln 2}} = \frac{f_e E}{2 \times \sqrt{2 \times \ln 2}}, \tag{7}$$

where σ is the standard deviation of the Gaussian function. The simulated spectrum $I_{sim}(E)$ is then convoluted with the Gaussian function.

The procedure for determining the IMFP is described as follows:

(1) Calculate the elastic scattering cross section and the DIIMFP of the material.
(2) Initialize arbitrary numerical values for the parameters β and γ.
(3) Calculate the backscattered electron energy distribution $I_{sim}(E_i)$ by a Monte Carlo simulation.
(4) Compute the potential energy U, defined as a measure of the difference between the simulated spectrum $I_{sim}(E_i)$ and the experimental spectrum $I_{exp}(E_i)$,

$$U = \sum_i \left(I_{sim}(E_i) - I_{exp}(E_i)\right)^2, \tag{8}$$

where the summation spans all measured data points in the energy range, typically from 200 or 300 eV to $E_0 - 100$ eV, with E_0 being the incident electron energy.
(5) Modify β and γ within a constrained range to generate an updated simulated spectrum $I'_{sim}(E_i)$ and the corresponding potential energy U', which is given by

$$U' = \sum_i \left(I'_{sim}(E_i) - I_{exp}(E_i)\right)^2. \tag{9}$$

(6) Evaluate the change in potential energy using $\Delta U = U' - U_{min}$, where U_{min} is the historical minimum. If $\Delta U < 0$, update the optimal parameters to the modified parameters β and γ and set $U_{min} = U'$.
(7) Repeat steps (5) and (6) until U_{min} converges below a predefined threshold or the maximum iteration count is reached. The optimal parameters β and γ, which minimize the difference between the simulated and experimental spectra, are then substituted into Eq. (5) to determine the IMFP of the material.

RESULTS AND DISCUSSION

We have determined the IMFPs from BES for 25 targets [C (graphite), Mg, Al (100), Al (111), Si, Ti, V, Cr, Fe, Co, Ni, Cu (100), Cu (110), Cu (111), Mo, Ru, Rh, Ag, Sn, W, Re, Ir, Pt, Au, and Bi] using the DIIMFPs calculated from both optical ELFs from the literature[47] and artificial ELFs. As illustrated in Fig. 3 for cobalt, the simulated energy spectrum obtained using the DIIMFP derived from the optical ELF shows excellent agreement with the experimental spectrum. Similarly, an agreement is also achieved with the artificial ELF for other materials such as Fe, Mo, Ir, Pt, and so on, as shown in Fig. 4. Figure 5 presents the corresponding IMFP curves extracted from energy spectra at the ten incident electron energies ranging from 400 to 5000 eV, along with the averaged values obtained through curve fitting.

The observed differences at Auger peaks [Figs. 3(c) and 3(d)] are expected, as our model does not account for Auger electron generation. This simplification is justified because Auger processes primarily contribute to peak features rather than the continuous background spectrum of backscattered electrons and consequently have negligible influence on the IMFP determination from spectrum shape analysis.

Our analysis focuses on the backscattered electron spectrum in the energy range of E_{min} to E_{max}, where E_{min} is 200 or 300 eV and E_{max} is $E_0 - 100$ eV. All reported IMFPs then correspond to this defined energy range. For the cobalt sample, ten independent electron energy spectra were acquired at different incident energies, each producing a distinct IMFP curve (scattered data points in Fig. 5). The final IMFP parameters were determined through a systematic two-step analytical process: (1) averaging individual IMFP curves across the 200–5000 eV range to obtain a composite curve and (2) a linear regression analysis based on Eq. (5). This fitting procedure yielded the characteristic IMFP parameters through the slope β and intercept $\beta \ln \gamma$ of the Fano plot, where $E[E_p^2 \lambda]^{-1}$ is plotted against $\ln E$. The experimental conditions and the derived IMFP parameters are summarized in Table I.

Similarly, the IMFPs for other materials are determined. Table II lists the IMFP parameters β and γ derived from the optical ELF data for the 25 elemental materials. The sources of these optical ELF data are shown in Table 2 of Ref. 47. The same analytical procedure was applied to artificial ELFs, and the resulting IMFP parameters are given in Table III.

Figure 6 presents a comparison of the IMFPs for Co, Ni, Cu (110), and W, calculated using different methods, along with the experimental and theoretical IMFP data from the literature. For clarity, the following nomenclature is adopted: Optical_IMFP: results derived from BES with the optical ELF; Artificial_IMFP: results derived from BES with the artificial ELF; FPA_IMFP:

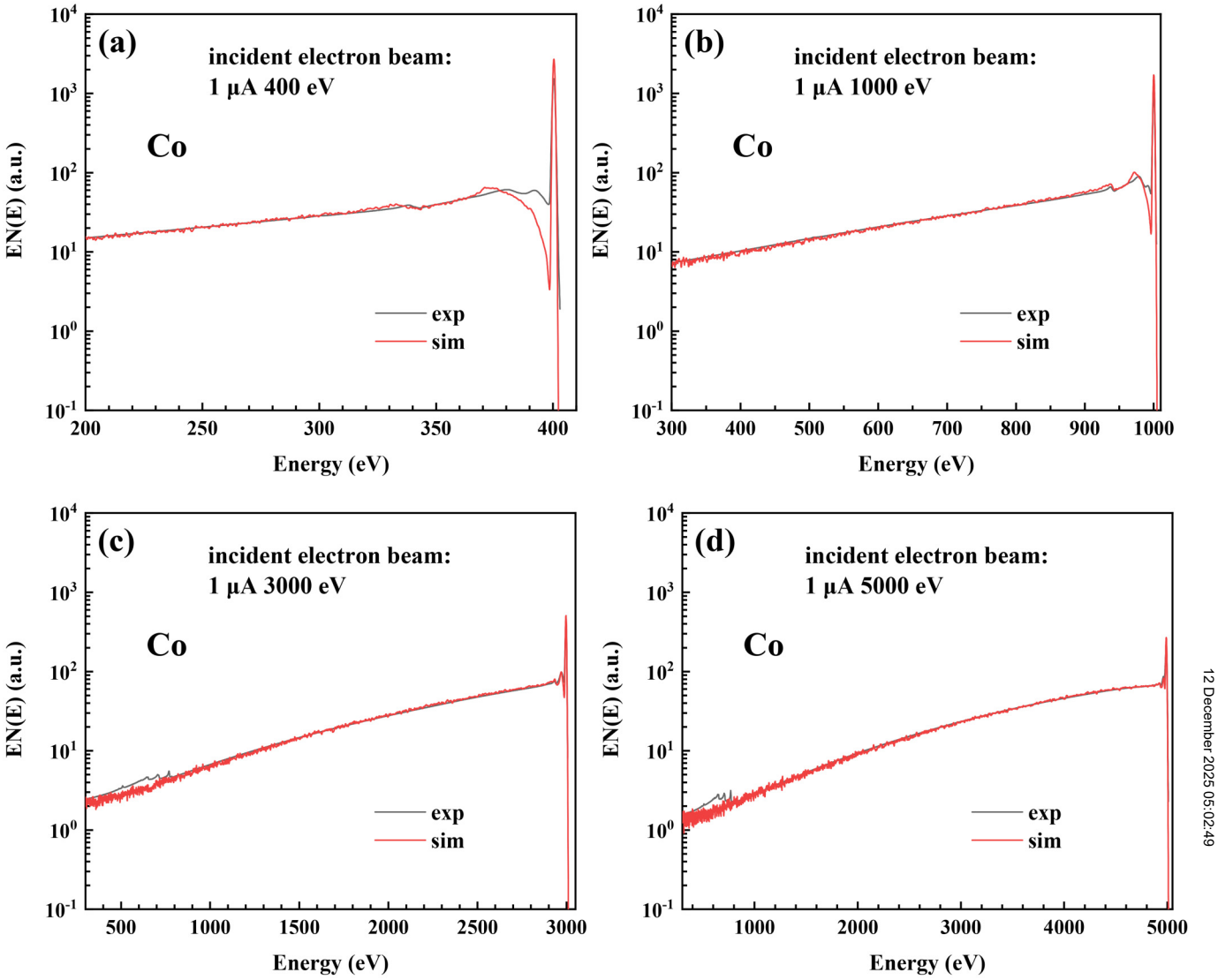

FIG. 3. Comparison between the simulated (red) and experimental (black) backscattered electron spectra for cobalt (Co) at primary electron energies of (a) 400 eV, (b) 1000 eV, (c) 3000 eV, and (d) 5000 eV. The incident electron beam current was maintained at 1 μA for all measurements. The DIIMFP is derived from the optical ELF.

IMFPs calculated using the FPA method;[27] and TPP_IMFP: IMFPs calculated using the TPP-2M formula.[47]

For cobalt [Fig. 6(a)], the Optical_IMFP and Artificial_IMFP exhibit excellent agreement with each other and closely match both FPA_IMFP and TPP_IMFP. In the case of copper [Fig. 6(c)] and tungsten [Fig. 6(d)], Optical_IMFP and Artificial_IMFP are consistent but diverge from FPA_IMFP and TPP_IMFP. For nickel, as can be observed from both Fig. 6(b) and Table IV, the results obtained by the BES method not only differ significantly from FPA_IMFP and TPP_IMFP but also reveal considerable discrepancies between Optical_IMFP and Artificial_IMFP.

Further comparison with IMFP data from the literature[5,7,8,50–63] indicates that notable variations exist among measurements obtained by different researchers and/or methods. We found that in the EPES method, the choice of reference materials significantly influences the results. For instance, in the IMFP measurements of Co and Ni, it can be observed that the IMFP values obtained by Krawczyk *et al.*[50] and Beilschmidt *et al.*[54] using different reference materials present considerable differences. In the case of Co, the Krawczyk_Pd (using Pd as the reference sample) IMFP values are higher than those obtained by the BES method, whereas the Krawczyk_Al (using Al as the reference sample) IMFP

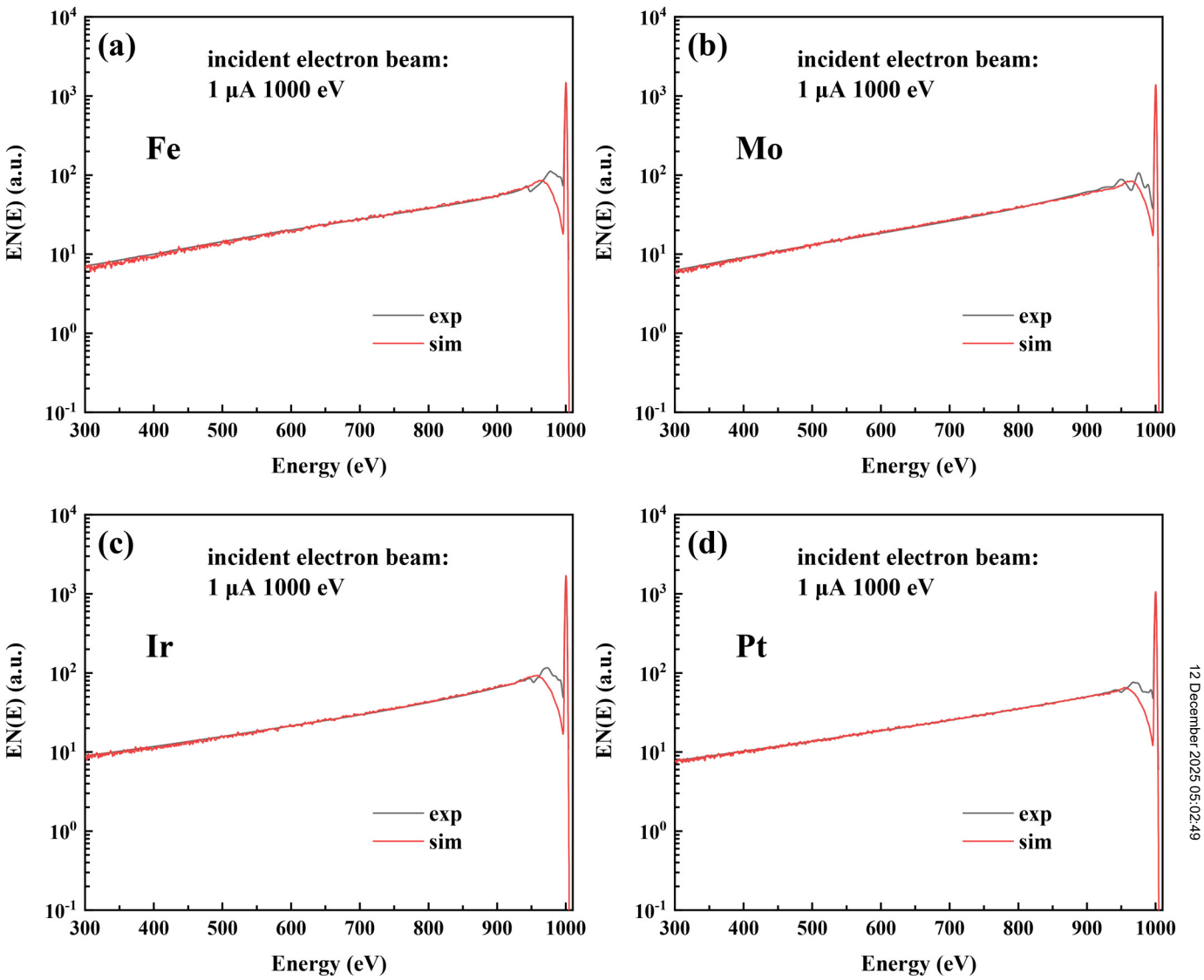

FIG. 4. Comparison between the simulated (red) and experimental (black) backscattered electron spectra for (a) Fe, (b) Mo, (c) Ir, and (d) Pt at the primary electron energy of 1000 eV. The incident electron beam current was maintained at 1 μA for all measurements. The DIIMFPs are derived from the artificial ELFs.

values are lower than the BES results. The results of Werner *et al.*[8,51] tend to converge with the present values at high energies. For Ni, the results of Nagatomi and Goto[53] and Beilschmidt *et al.*[54] using Pt (Beilschmidt_Pt) and Au (Beilschmidt_Au) as reference samples align closely with Optical_IMFP, whereas Beilschmidt_Al IMFP data exhibit close agreement with the Artificial_IMFP results. In contrast, the data of Gergely *et al.*[55] and Werner[56] show better consistency with the TPP-2M[47] and FPA[27] predictions. For Cu, the IMFP measurements by Doliński *et al.*[57,58] are in close agreement with the BES results. However, another set of data published by Doliński *et al.*[59] aligns more closely with Werner's fitting curve.[51] Similarly, the measurements from Tanuma *et al.*[60] show excellent consistency with Werner's fitting curve.[51] The IMFP data points reported by Lesiak *et al.*[61] nearly coincide with the FPA_IMFP[27] values, while the results by Gergely *et al.*[62] exhibit better agreement with the TPP_IMFP values.[47] The measurements by Tanuma *et al.*[7] fall between the results obtained by the BES method and the FPA method.[27] Notably, Jablonski's measurement result[5] lies precisely at the intersection of the TPP_IMFP[47] and Werner's curve.[51] For W, the results of Gergely *et al.*[62] show better agreement with FPA_IMFP and TPP_IMFP, while those of Werner *et al.*[8,51] and Tanuma *et al.*[7] exhibit closer consistency with the BES

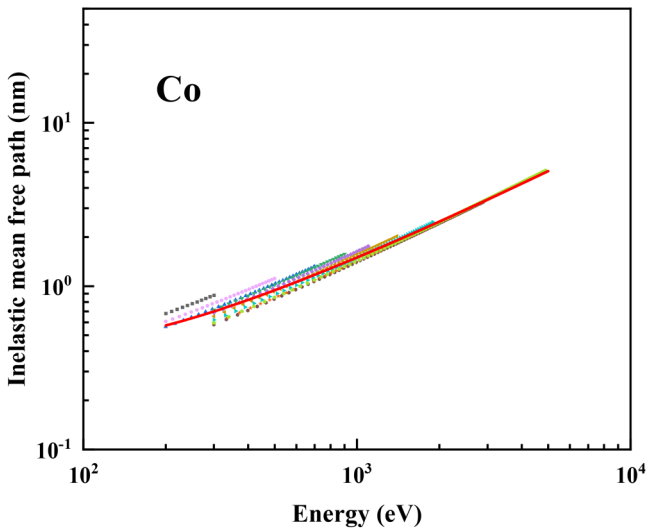

FIG. 5. IMFPs of Co derived using the BES method at ten primary electron energies (scattered data points). The red solid line represents the averaged IMFP by fitting the ten individual results.

results. Notably, Lesiak's measured IMFP values[63] are lower than the other data sets.

Based on the above analysis, it can be observed that the IMFPs of materials obtained by different theoretical and experimental methods exhibit certain differences. Even with the same EPES method, the selection of different reference samples leads to variations in results. The diversity of measurement uncertainty sources—including measurement methods, instruments, and approximations in theoretical models—makes it very difficult to assess the accuracy of IMFP results.

Given that the most comprehensive IMFP data sets currently available are derived from FPA_IMFP and TPP_IMFP, we have conducted a focused comparison between these reference data and the IMFP values extracted using the BES method.

A data deviation analysis of the IMFPs extracted for these 25 targets was conducted by comparing the IMFPs obtained using our method with those derived using the FPA method[27] and the TPP-2M formula.[47] The root-mean-square (RMS) deviation between the two sets of IMFP data, A and B, is defined as follows:

$$RMS_{A,B} = 100 \times \sqrt{\frac{1}{n}\sum_{i=1}^{n}\left(\frac{\lambda_{\mathrm{in},A}(E_i) - \lambda_{\mathrm{in},B}(E_i)}{\lambda_{\mathrm{in},B}(E_i)}\right)^2}, \quad (10)$$

where E_i represents the electron energy. In our comparison, the IMFP results obtained using the BES method are designated as set A and the IMFP data for comparison (either the FPA or the

TABLE I. Summary of the experimental conditions and the derived IMFP parameter values for Co using the BES method.

No.	E_0 (eV)	$E_{\min}$ (eV)	$E_{\max}$ (eV)	β (eV^{-1} nm^{-1})	γ (eV^{-1})
1	400.25	200.00	300.25	0.112 09	0.062 10
2	600.30	200.00	500.30	0.118 72	0.062 10
3	800.10	200.00	700.10	0.127 39	0.062 10
4	1000.00	300.00	900.00	0.126 06	0.065 57
5	1199.80	300.00	1099.80	0.135 46	0.065 14
6	1499.60	300.00	1399.60	0.138 66	0.068 05
7	1998.80	300.00	1898.80	0.139 81	0.074 14
8	2996.50	300.00	2896.50	0.141 98	0.073 61
9	3993.50	300.00	3893.50	0.146 49	0.071 77
10	4989.50	300.00	4889.50	0.145 74	0.072 16
Mean	…	200.00	4889.50	0.172 38	0.031 42

TABLE II. List of the parameters β and γ in the TPP-2M formula for 25 elemental solids derived using the BES method and optical ELFs.

Element	β (eV^{-1} nm^{-1})	γ (eV^{-1})	Element	β (eV^{-1} nm^{-1})	γ (eV^{-1})
Ag	0.229 36	0.026 99	Mg	0.545 20	0.153 20
Al (100)	0.412 57	0.067 20	Mo	0.369 51	0.072 11
Al (111)	0.335 52	0.296 33	Ni	0.164 91	0.039 79
Au	0.275 38	0.042 01	Pt	0.276 19	0.052 00
Bi	0.711 88	0.033 39	Re	0.362 08	0.021 31
C (graphite)	0.186 50	0.059 46	Rh	0.249 86	0.061 25
Co	0.172 38	0.031 42	Ru	0.428 75	0.024 59
Cr	0.264 14	0.065 68	Si	0.274 29	0.197 51
Cu (100)	0.172 10	0.013 07	Sn	0.580 59	0.030 26
Cu (110)	0.124 88	0.187 98	Ti	0.486 02	0.042 78
Cu (111)	0.128 74	0.080 24	V	0.332 21	0.043 60
Fe	0.241 91	0.023 59	W	0.478 12	0.025 67
Ir	0.284 90	0.027 66			

TABLE III. List of the parameters β and γ in the TPP-2M formula for 25 elemental solids derived using the BES method and artificial ELFs.

Element	β (eV^{-1} nm^{-1})	γ (eV^{-1})	Element	β (eV^{-1} nm^{-1})	γ (eV^{-1})
Ag	0.273 09	0.025 74	Mg	0.591 53	0.129 70
Al (100)	0.363 32	0.069 89	Mo	0.366 03	0.065 56
Al (111)	0.289 24	0.360 82	Ni	0.204 98	0.065 61
Au	0.264 64	0.042 76	Pt	0.277 49	0.043 06
Bi	0.873 69	0.027 48	Re	0.344 31	0.020 61
C (graphite)	0.187 66	0.063 50	Rh	0.240 64	0.057 39
Co	0.176 02	0.028 87	Ru	0.408 30	0.022 33
Cr	0.261 48	0.053 34	Si	0.255 77	0.232 33
Cu (100)	0.183 82	0.012 00	Sn	0.757 16	0.024 06
Cu (110)	0.138 54	0.129 39	Ti	0.476 30	0.041 74
Cu (111)	0.145 05	0.054 82	V	0.357 45	0.036 51
Fe	0.250 22	0.018 19	W	0.473 25	0.024 72
Ir	0.275 19	0.025 10			

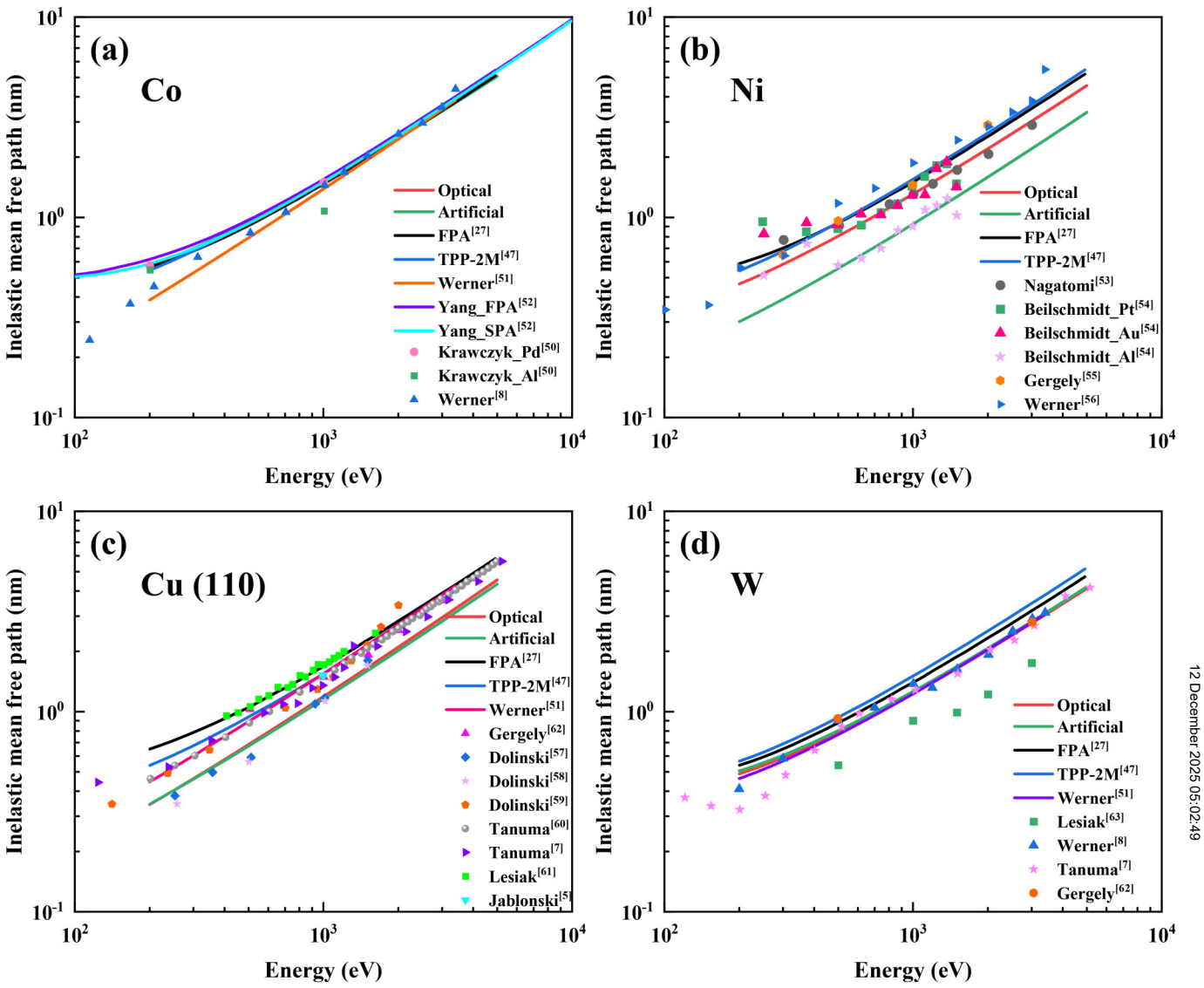

FIG. 6. Comparison of IMFPs for: (a) Co, (b) Ni, (c) Cu (110), and (d) W, calculated using different methods: BES with the optical ELF (red), BES with the artificial ELF (green), the FPA model (black),[27] and the TPP-2 M formula (blue).[47] The experimental and theoretical IMFP data are taken from the literature.[5,7,8,27,47,50–63]

TPP-2M data) are designated as set B. Table IV lists the *RMS* between the IMFPs obtained in this study and the corresponding values derived using the FPA method and the TPP-2M formula reported in the literature.[27,47]

The results demonstrate that for most materials except Ni, the *RMS* differences between the obtained two sets of IMFPs and those calculated using either the FPA method or the TPP-2M formula are relatively small. This indicates that the approach of extracting IMFPs from BES is basically practicable. The proposed scheme exhibits strong extensibility—by employing a universal approach based on the artificial ELF, only the material's chemical formula and density are required for modeling electron inelastic scattering to derive the IMFP from BES. The artificial ELF has two key characteristics: (1) it satisfies the sum rules and (2) its ELF shape may be quite different from the realistic ELF. The first feature offers an advantage by ensuring that the modeling of energy loss in electron inelastic scattering in a Monte Carlo simulation does not lose too much accuracy due to the second feature, and these inaccuracies would be smeared out in the multiple inelastic scattering events of backscattered electrons. For certain materials (e.g., Au, Cr, Fe, Mg, Mo, Pt, Rh, Ru, and W), the artificial ELFs yield IMFPs that are in better agreement with FPA_IMFP and TPP_IMFP results, as they satisfy the sum rules.

TABLE IV. *RMS* between the IMFPs derived in this work and those obtained using the FPA method[27] and the TPP-2M formula.[47]

	RMS[a]		*RMS*[b]		
Element	FPA	TPP-2M	FPA	TPP-2M	*RMS*[c]
Ag	4.69	4.60	11.44	13.79	14.67
Al (100)	7.56	2.69	20.91	9.82	12.45
Al (111)	6.56	13.12	10.79	5.95	12.03
Au	20.89	12.67	18.13	9.66	3.53
Bi	2.82	11.02	12.22	22.79	13.36
C (graphite)	15.59	21.52	12.92	23.32	2.33
Co	1.51	4.38	2.25	4.67	1.06
Cr	20.33	24.30	15.00	19.24	6.82
Cu (100)	16.39	29.02	17.11	28.92	3.11
Cu (110)	32.19	24.96	33.84	26.78	3.03
Cu (111)	20.87	12.25	22.37	13.98	3.22
Fe	16.70	14.62	13.17	12.09	7.56
Ir	6.43	1.69	1.85	8.32	7.08
Mg	17.40	7.06	11.99	2.15	4.59
Mo	24.71	29.49	22.15	27.09	3.44
Ni	14.58	15.64	39.98	40.74	29.84
Pt	25.00	17.01	21.28	12.86	5.12
Re	8.85	5.41	15.60	10.68	6.48
Rh	18.35	23.42	13.79	19.14	5.63
Ru	33.99	36.80	28.43	31.43	8.74
Si	4.57	5.44	7.00	9.19	3.98
Sn	8.65	10.01	11.38	12.25	17.30
Ti	3.12	17.96	4.47	15.74	2.78
V	7.26	14.58	9.34	16.48	2.55
W	11.76	17.90	9.77	16.05	2.39
Mean	14.03	15.10	15.49	16.53	7.32

[a]set A = Optical_IMFP; set B = FPA_IMFP or TPP_IMFP.
[b]set A = Artificial_IMFP; set B = FPA_IMFP or TPP_IMFP.
[c]set A = Optical_IMFP; set B = Artificial_IMFP.

From the rightmost column of Table IV, it is evident that different ELFs, or different energy loss distributions, do not significantly alter the final IMFP results. The bottom row of Table IV indicates that the average *RMS* value between Optical_IMFP and Artificial_IMFP is as low as 7.32%. It should be noted that this does not imply the difference introduced by the artificial ELF is 7.32%. For example, Sn shows a high *RMS* value of 17.30% between Optical_IMFP and Artificial_IMFP. However, their deviations from the reference standards are much lower: 8.65% and 11.38% from FPA_IMFP and 10.01% and 12.25% from TPP_IMFP, respectively.

It can be observed that the *RMS* differences between the current study results and those using the FPA method and the TPP-2M formula are, on average, around 15%. Although the differences reach approximately 30% for some materials [e.g., Ru, Cu (110), Cu (100), Mo, and Ni], the results obtained using the BES method are quite satisfactory overall, considering that each method may have inherent uncertainty and result in deviation from the true values.

CONCLUSION

In this work, we have demonstrated a novel method for determining the electron IMFP by analyzing the backscattered electron spectrum (BES). This approach offers distinct advantages over conventional techniques. Specifically, it is less sensitive to surface conditions than methods based on secondary electrons and avoids the complex surface excitation corrections required in EPES analysis. While the resulting IMFP values do not necessarily represent an improvement in accuracy over established theoretical models, they show good agreement, with average differences of ∼15% from FPA and TPP-2M predictions for 25 different elemental solids. This consistency validates the BES method as a powerful addition to the existing analytical tools for IMFP determination. Crucially, our work transforms the continuous background in electron spectra, a signal that is typically discarded, into a valuable source for quantitative material analysis. The method is applicable for electron energies above ∼200 eV, where the influence of secondary electrons is negligible.

ACKNOWLEDGMENTS

B. Da acknowledges JSPS KAKENHI (No. JP21K14656) and the Kurata Grants from the Hitachi Global Foundation and from the Iketani Science & Technology Foundation. The authors in ZJU acknowledge financial support by the National Key R&D Program of China under Grant No. 2022YFB4401602 and the 111 Project under Grant No. B16042. They thank Professor K. Goto for his experimental support and assistance. They also extend their gratitude to Dr. H. M. Li and the supercomputing center of USTC for parallel computing support.

AUTHOR DECLARATIONS

Conflict of Interest

The authors have no conflicts to disclose.

Author Contributions

Jiamin Gong: Data curation (equal); Formal analysis (equal); Investigation (equal); Methodology (equal); Validation (equal); Visualization (equal); Writing – original draft (equal). **Lihao Yang:** Data curation (equal); Formal analysis (equal); Investigation (equal); Methodology (equal); Software (equal). **Hideki Yoshikawa:** Resources (equal); Supervision (equal). **Shigeo Tanuma:** Conceptualization (equal); Resources (equal); Supervision (equal). **Bo Da:** Conceptualization (equal); Funding acquisition (equal); Project administration (equal); Resources (equal); Supervision (equal). **Chuanhong Jin:** Funding acquisition (equal); Project administration (equal); Resources (equal); Supervision (equal); Writing – review & editing (equal). **Zejun Ding:** Conceptualization (equal); Funding acquisition (equal); Methodology (equal); Project administration (equal); Resources (equal); Software (equal); Supervision (equal); Writing – review & editing (equal).

DATA AVAILABILITY

The data that support the findings of this study are available from the corresponding authors upon reasonable request.

REFERENCES

[1]C. R. Brundle and A. D. Baker, *Electron Spectroscopy: Theory, Techniques and Applications* (Academic Press, New York, 1981).
[2]D. Briggs and M. P. Seah, "Practical surface analysis," in *Auger and X-Ray Photoelectron Spectroscopy* (Wiley, Chichester, 1990), Vol. 1.
[3]C. J. Powell and A. Jablonski, J. Phys. Chem. Ref. Data **28**, 19 (1999).
[4]B. Lesiak, A. Jablonski, Z. Prussak, and P. Mrozek, Surf. Sci. **223**, 213 (1989).
[5]A. Jablonski, B. Lesiak, and G. Gergely, Phys. Scr. **39**, 363 (1989).
[6]G. Gergely, Prog. Surf. Sci. **71**, 31 (2002).
[7]S. Tanuma, T. Shiratori, T. Kimura, K. Goto, S. Ichimura, and C. J. Powell, Surf. Interface Anal. **37**, 833 (2005).
[8]W. S. M. Werner, C. Tomastik, T. Cabela, R. Gerald, and H. Störi, Surf. Sci. **470**, L123 (2000).
[9]B. Lesiak, J. Zemek, and J. Houdkova, Polymer **49**, 4127 (2008).
[10]J. Zemek, P. Jiricek, B. Lesiak, and A. Jablonski, Surf. Sci. **531**, L335 (2003).
[11]A. Jablonski, Surf. Interface Anal. **37**, 1035 (2005).
[12]M. P. Seah and W. Dench, Surf. Interface Anal. **1**, 2 (1979).
[13]A. Jablonski and S. Tougaard, J. Vac. Sci. Technol. A **8**, 106 (1990).
[14]C. J. Powell, J. Vac. Sci. Technol. A **4**, 1532 (1986).
[15]S. Suryani, Heryanto, and D. Tahir, Surf. Interface Anal. **52**, 16 (2020).
[16]W. S. M. Werner, V. Astašauskas, O. Ridzel, A. Bellissimo, and M. Stöger-Pollach, Surf. Interface Anal. **57**, 445 (2025).
[17]F. Yubero, J. M. Sanz, J. F. Trigo, E. Elizalde, and S. Tougaard, Surf. Interface Anal. **22**, 124 (1994).
[18]T. Nagatomi and K. Goto, Phys. Rev. B **75**, 235424 (2007).
[19]J. Gong, K. Tőkési, X. Liu, B. Da, H. Yoshikawa, S. Tanuma, and Z. Ding, Results Phys. **51**, 106609 (2023).
[20]L. H. Yang, M. Menyhárd, A. Sulyok, K. Tőkési, and Z. J. Ding, Appl. Surf. Sci. **456**, 999 (2018).
[21]S. Tanuma, C. J. Powell, and D. R. Penn, Surf. Interface Anal. **11**, 577 (1988).
[22]C. J. Powell, Surf. Sci. **44**, 29 (1974).
[23]Y. Sun, H. Xu, B. Da, S. F. Mao, and Z. J. Ding, Chin. J. Chem. Phys. **29**, 663 (2016).
[24]C. D. Denton, I. Abril, R. Garcia-Molina, J. C. Moreno-Marín, and S. Heredia-Avalos, Surf. Interface Anal. **40**, 1481 (2008).
[25]U. Fano, Phys. Rev. **103**, 1202 (1956).
[26]A. J. Glick and R. A. Ferrell, Ann. Phys. **11**, 359 (1960).
[27]H. Shinotsuka, S. Tanuma, C. J. Powell, and D. R. Penn, Surf. Interface Anal. **47**, 871 (2015).
[28]D. R. Penn, Phys. Rev. B **35**, 482 (1987).
[29]B. Da, Y. Sun, S. Mao, Z. Zhang, H. Jin, H. Yoshikawa, S. Tanuma, and Z. J. Ding, J. Appl. Phys. **113**, 214303 (2013).
[30]H. Xu, B. Da, J. Tóth, K. Tőkési, and Z. J. Ding, Phys. Rev. B **95**, 195417 (2017).
[31]L. H. Yang, K. Tőkési, J. Tóth, B. Da, H. M. Li, and Z. J. Ding, Phys. Rev. B **100**, 245209 (2019).
[32]L. H. Yang, J. M. Gong, A. Sulyok, M. Menyhárd, G. Sáfrán, K. Tőkési, B. Da, and Z. J. Ding, Phys. Chem. Chem. Phys. **23**, 25335 (2021).
[33]Z. Li, J. M. Gong, Y. Harada, B. Da, R. G. Zeng, and Z. J. Ding, Results Phys. **56**, 107247 (2024).
[34]T. F. Yang, J. Tóth, K. Tőkési, R. G. Zeng, and Z. J. Ding, Vacuum **223**, 113097 (2024).
[35]J. M. Gong, X. Liu, L. H. Yang, A. Sulyok, Z. Baji, V. Kis, K. Tőkési, R. G. Zeng, G. J. Fang, J. B. Gong, X. D. Xiao, B. Da, and Z. J. Ding, J. Alloys Compd. **1005**, 175744 (2024).
[36]X. H. Zhou, J. M. Gong, Z. Li, A. Sulyok, M. Menyhard, Y. Harada, B. Da, R. G. Zeng, K. Tőkési, and Z. J. Ding, J. Phys. Chem. C **129**, 6524 (2025).
[37]O. Y. Ridzel, V. Astašauskas, and W. S. M. Werner, J. Electron Spectrosc. Relat. Phenom. **241**, 146824 (2020).
[38]S. Tanuma, C. J. Powell, and D. R. Penn, Surf. Interface Anal. **21**, 165 (1994).
[39]K. Goto, N. Sakakibara, Y. Takeichi, Y. Numata, and Y. Sakai, Surf. Interface Anal. **22**, 75 (1994).
[40]Y. Takeichi and K. Goto, Surf. Interface Anal. **25**, 17 (1997).
[41]A. Hussain, L. H. Yang, Y. B. Zou, S. F. Mao, B. Da, H. M. Li, and Z. J. Ding, J. Appl. Phys. **127**, 125304 (2020).
[42]N. F. Mott, Proc. R. Soci. Lond. Ser. A **124**, 425 (1929).
[43]H. Shinotsuka, S. Tanuma, C. J. Powell, and D. R. Penn, Surf. Interface Anal. **51**, 427 (2019).
[44]B. L. Henke, E.M. Gullikson, and J.C. Davis, At. Data Nucl. Data Tables **54**, 181 (1993).
[45]D. E. Cullen, J. H. Hubbell, and L. Kissel, *EPDL97: The Evaluated Photon Data Library* (Lawrence Livermore National Laboratory, 1997), available at https://www.osti.gov/biblio/295438.
[46]S. Tanuma, C. J. Powell, and D. R. Penn, J. Electron Spectrosc. Relat. Phenom. **62**, 95 (1993).
[47]S. Tanuma, C. J. Powell, and D. R. Penn, Surf. Interface Anal. **43**, 689 (2011).
[48]S. Tanuma, C. J. Powell, and D. R. Penn, Surf. Interface Anal. **17**, 911 (1991).
[49]X. Liu, Z. Hou, D. Lu, B. Da, H. Yoshikawa, S. Tanuma, Y. Sun, and Z. J. Ding, Sci. Technol. Adv. Mater. **20**, 1090 (2019).
[50]M. Krawczyk, L. Zommer, B. Lesiak, and A. Jablonski, Surf. Interface Anal. **25**, 356 (1997).
[51]W. S. M. Werner, C. Tomastik, T. Cabela, G. Richter, and H. Störi, J. Electron Spectrosc. Relat. Phenom. **113**, 127 (2001).
[52]L. H. Yang, K. Tőkési, B. Da, and Z. J. Ding, Eur. Phys. J. D **73**, 1 (2019).
[53]T. Nagatomi and K. Goto, Appl. Phys. Lett. **87**, 224107 (2005).
[54]H. Beilschmidt, I. S. Tiliuin, and W. S. M. Werner, Surf. Interface Anal. **22**, 120 (1994).
[55]G. Gergely, M. Menyhard, S. Gurban, J. Toth, and D. Varga, Surf. Interface Anal. **36**, 1098 (2004).
[56]W. S. M. Werner, Surf. Sci. **601**, 2125 (2007).
[57]W. Doliński, S. Mróz, and M. Zagórski, Surf. Sci. **200**, 361 (1988).
[58]W. Doliński, H. Nowicki, and S. Mróz, Surf. Interface Anal. **11**, 229 (1988).
[59]W. Doliński, S. Mróz, J. Palczyński, B. Gruzza, P. Bondot, and A. Porte, Acta Phys. Pol. A **81**, 193 (1992).
[60]S. Tanuma, H. Yoshikawa, N. Okamoto, and K. Goto, J. Surf. Anal. **15**, 195 (2008).
[61]B. Lesiak, A. Jablonski, J. Zemek, and P. Jiricek, Surf. Interface Anal. **26**, 400 (1998).
[62]G. Gergely, M. Menyhard, K. Pentek, A. Sulyok, A. Jablonski, B. Lesiak, and C. Daroczi, Vacuum **46**, 591 (1995).
[63]B. Lesiak, A. Jablonski, and G. Gergely, Vacuum **40**, 67 (1990).